ChemBioChem

Research Article
doi.org/10.1002/cbic.202400084

Chemistry Europe
European Chemical Societies Publishing

www.chembiochem.org

Enhancing PET Degrading Enzymes: A Combinatory Approach

Yvonne Joho,[a, b, c] Santana Royan,[a] Alessandro T. Caputo,[a] Sophia Newton,[a] Thomas S. Peat,[d] Janet Newman,[d] Colin Jackson,[b, e, f] and Albert Ardevol*[a, c]

Plastic waste has become a substantial environmental issue. A potential strategy to mitigate this problem is to use enzymatic hydrolysis of plastics to depolymerize post-consumer waste and allow it to be reused. Over the last few decades, the use of enzymatic PET-degrading enzymes has shown promise as a great solution for creating a circular plastic waste economy. *Ps*PETase from *Piscinibacter sakaiensis* has been identified as an enzyme with tremendous potential for such applications. But to improve its efficiency, enzyme engineering has been applied aiming at enhancing its thermal stability, enzymatic activity, and ease of production. Here, we combine different strategies such as structure-based rational design, ancestral sequence reconstruction and machine learning to engineer a more highly active Combi-PETase variant with a melting temperature of 70 °C and optimal performance at 60 °C. Furthermore, this study demonstrates that these approaches, commonly used in other works of enzyme engineering, are most effective when utilized in combination, enabling the improvement of enzymes for industrial applications.

Introduction

The escalating global issue of plastic waste accumulation and its improper disposal practices have led to significant environmental and health concerns. The adverse impacts of plastic pollution on ecosystems are being increasingly recognized[1] and recent discoveries highlight how the ingestion of microplastics pose potential risks to human health as well.[2] There is a critical need to address these global challenges and to minimize the ecological harm caused by plastic waste. Worldwide, only 9% of plastic waste gets recycled,[3] mostly by thermomechanical methods that result in a less valuable product. "Advanced recycling" is the conversion of plastic waste into monomers or other valuable raw materials by means of cracking, gasification or depolymerization, excluding energy recovery and incineration. The resulting materials can be used to manufacture recycled products of high quality, enabling a truly circular economy for plastic materials. Amongst the advanced recycling technologies, enzymatic depolymerization offers a relatively simple and cost-effective solution for easily hydrolysable plastics such as polyethylene terephthalate (PET).[4] Considerable progress has been achieved since the first reports of enzymatic PET degradation using *Thermobifida fusca* cutinase.[5] A breakthrough was achieved by Yoshida et al. in 2016 with the discovery of the bacterium *Ideonella sakaiensis* (now currently known as *Piscinibacter sakaiensis*), the first microorganism that showed ability to use PET as a primary carbon source[6] and which was later engineered to turn non-biodegradable PET into biodegradable polyhydroxyalkanoates (PHA).[7,8]

P. sakaiensis breaks down the polyester chains using a PET hydrolase enzyme (*Ps*PETase aka *Is*PETase, basonym *Ideonella sakaiensis)*, producing the monomers terephthalic acid (TPA) and mono-2-hydroxyethyl terephthalate (MHET). Subsequently, another exo-hydrolase enzyme (MHETase) cleaves the ester bond of MHET, yielding TPA and ethylene glycol (EG). The closest homologs of *Ps*PETase are the cutinase enzymes, a family of natural polyester hydrolases which includes other enzymes that have shown promiscuous activity against PET. Some of these enzymes are more active at higher temperatures than *Ps*PETase (e.g. LCC cutinase,[9] TfH,[5] *F. solani* cutinase (FsC)[10]) but *Ps*PETase is the most efficient enzyme at room temperature.[6] Depolymerization of PET for viable recycling and bioremediation applications requires engineering of the naturally occurring enzymes to improve their biophysical and

[a] *Y. Joho, S. Royan, A. T. Caputo, S. Newton, A. Ardevol*
Manufacturing, Commonwealth Scientific and Industrial Research Organisation, Clayton, Victoria 3168, Australia
E-mail: albert.ardevolgrau@csiro.au

[b] *Y. Joho, C. Jackson*
Research School of Chemistry, Australian National University, Canberra, ACT 2601, Australia

[c] *Y. Joho, A. Ardevol*
CSIRO Advanced Engineering Biology Future Science Platform, GPO Box 1700, Canberra, ACT 2601, Australia

[d] *T. S. Peat, J. Newman*
School of Biotechnology & Biomolecular Sciences, University of New South Wales, Sydney, NSW 2052, Australia

[e] *C. Jackson*
ARC Centre of Excellence for Innovations in Peptide & Protein Science, Research School of Chemistry, Australian National University, Canberra, ACT 2601, Australia

[f] *C. Jackson*
ARC Centre of Excellence for Innovations in Synthetic Biology, Research School of Chemistry, Australian National University, Canberra, ACT 2601, Australia

Supporting information for this article is available on the WWW under https://doi.org/10.1002/cbic.202400084

biochemical properties such as: thermal stability,[11][12] higher turnover rates,[13] and substrate specificity.[14,15,16] Indeed, without exception, all the natural and engineered variants of *Ps*PETase and other enzymes are far more active with low-crystalline (lc-PET) rather than with high-crystalline PET (hc-PET).[17,18,19,20] This hinders their industrial application and/or requires costly pretreatment of the substrate before the catalytic hydrolysis step.[4] Additionally, the efficient production of the enzyme in large quantities is crucial for large-scale industrial applications. It is essential to assess early these critical parameters for upscaling enzyme-based PET depolymerization when engineering a new variant of a PETase enzyme.[21]

Even for a small protein such as *Ps*PETase, which consists of 290 amino acids, the number of possible amino acid mutations, deletions or insertions to the wild type sequence is overwhelming. Therefore, the focus of enzyme engineering methods is to provide guidance in identifying beneficial variants with desirable traits. Various strategies have been applied to engineer better variants of *Ps*PETase, with remarkable results.[18] Typical strategies include structure- or mechanism-based methods (e.g. rational design),[11] bioinformatics-based methods (e.g. Ancestral Sequence Reconstruction),[22,23] directed evolution[24] or ML/AI-based methods (e.g. deep learning,[25] and graph convolutional networks).[26] Structure-based rational design strategies, based on a fundamental understanding of the role of individual amino acids on the biochemical and biophysical properties of the enzyme, have produced variants of *Ps*PETase with increases of 10–30 °C in the melting temperature.[27,28] A good example of a *Ps*PETase variant developed by structure-based enzyme engineering is the work of Son *et al.* who created the ThermoPETase variant by: i) structural comparison with other homologous thermophilic enzymes such as *Tf*Cut2; and ii) optimizing hydrogen bond interactions to stabilize flexible regions based on the observed B-factor from X-ray structures.[11] ThermoPETase has been very important in the field and used as a starting point for further development using other techniques. Computational predictions of the enzyme properties can support rational enzyme engineering by providing a way to screen the possible variants *in silico*, increasing the number of variants that can be explored. An example of this is the DuraPETase variant which showed remarkably higher stability temperatures, elevated by 31 °C compared to the wild type.[12]

Ancestral sequence reconstruction (ASR) enables the prediction of the sequence of ancestral enzymes based on the multi-sequence alignment of extant variants. Without the need of structural information or understanding contribution of each amino acid substitution to the biophysical properties of the enzyme, the ASR approach produces enzymes that are often more thermostable, soluble and promiscuous.[29,30] These properties are very desirable in enzyme engineering and therefore ASR has been widely used for creating new functionality in enzymes and to improve their properties.[22] We recently applied ancestral sequence reconstruction to understand the evolutionary history of *Ps*PETase.[23] This resulted in the recreation of ancestral enzymes containing mutations which could not have been found by rational design methods, as they are not close to the active site nor their effect could have been predicted. However, because of their beneficial effects on the thermostability and protein yield, we have introduced them as part of the multi-methodological approach to obtain an improved *Ps*PETase variant.

Machine learning and deep learning methods have been applied to develop both novel plastic degrading enzymes as well as PET hydrolase variants. Although this is an emerging strategy with only a limited number of examples, a few remarkable studies have demonstrated the synergistic effect of combining ML/AI and rational design methods. For instance, FAST-PETase is a variant of *Ps*PETase that was developed combining two mutations from the rational-engineered ThermoPETase and three other mutations identified with MutCompute.[13] Similarly, MutCompute was applied to *Tf*Cut2 wild type cutinase to identify beneficial mutations and create an enhanced variant, which exhibited a 5.3-fold improved depolymerization of crystalline PET.[31]] Most recent examples include the adoption of machine learning-assisted prediction of the degrading activity of certain plastics[32] or the use of machine learning to guide the directed evolution of plastic degrading enzymes.[33]

This paper has applied different approaches such as structure-based design, ancestral sequence reconstruction and machine learning to engineer a new variant of *Ps*PETase. We show that each approach has unique benefits and limitations, and that they can be applied to complement each other in a combinatorial approach. We present a new enzyme (namely Combi-PETase) with improved properties that are critical for industrial applications.

Results and Discussion

Evaluation of PsPETase Variants

Using the wild type *Ps*PETase as our starting point, we have applied a combination of structure-based rational design, ancestral sequence reconstruction and machine learning approaches over six generations of engineering. We have characterized the PET hydrolytic activity, thermal stability and expression levels in *E. coli* of over 140 variants in an iterative process of improving the enzyme's properties. We determined the thermal stability of each variant by measuring the melting temperature using differential scanning fluorimetry (DSF) experiments and we used a fluorescence-based assay of TPA released to determine the PET hydrolytic activity (see methods).

Figure 1 shows the characterization of the best variants that were passed to the following generation, accumulating beneficial mutations in the process. The optimal temperature of the reaction was determined by measuring the enzymatic activity. For the best variant in each generation, we determined the optimal temperature of the reaction by measuring the activity over a range of temperatures (Figure 1A–C, Table 1). Our best variant (namely Combi-PETase or PETase^{ACCCETN}) contains seven accumulated mutations obtained from different enzyme engi-

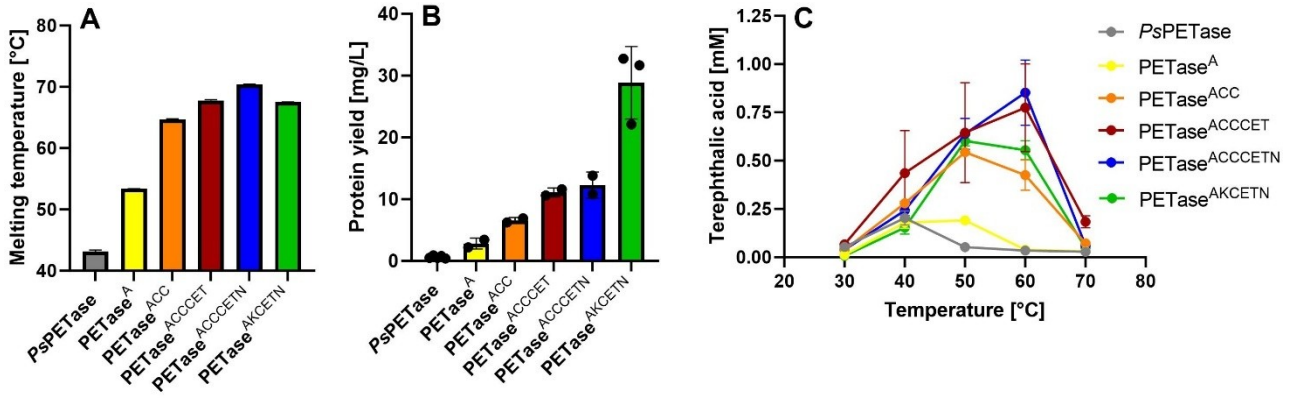

Figure 1. Screening parameters employed across PETase engineering generations. A Melting temperature measured by DSF recorded with six replicates. SD is represented as error bars. B Soluble protein yield obtained after purification. C Enzymatic activity degrading hc-PET using 500 nM enzyme at temperatures between 30 to 70 °C. The reaction was performed in three replicates and at the corresponding temperature for one hour agitating at 1000 rpm.

Table 1. Summary of thermostability, activity, and soluble yield for selected engineered PETase variants. The melting temperature was determined by differential scanning fluorimetry (DSF). PET degradation activity was measured as concentration of released TPA products after incubating hc-PET substrate with 500 nM enzyme concentration at the enzyme's optimal temperature for one hour and shaking at 1000 rpm.

Variant/Approach	Mutations	Activity [TPA mM/1 h]	Tm [°C]	Protein Yield [mg/L]
*Ps*PETase	None	0.20 ± 0.04	43.2 ± 0.2	0.5
PETase^{A} RD (rational design)	D186A	0.19 ± 0.02	53.3 ± 0.1	2.9
PETase^{ACC} RD	D186A/N233C/S282C	0.54 ± 0.01	64.7 ± 0.1	6.6
PETase^{ACCCET} RD	ACC/A179C/S136E/ S214T	0.77 ± 0.2	68.6 ± 0.2	11.1
PETase^{ACCCETN} (Combi-PETase) RD + ASR	ACCCET/K95N	0.85 ± 0.2	70.4 ± 0.04	12.3
PETase^{AKCETN} RD + ASR + AI	D186A/N233K/A179C/S136E/S214T/K95N	0.56 ± 0.05	67.5 ± 0.1	29

neering approaches and displays a 27 °C increase in melting temperature, with an optimal reaction temperature of 60 °C.

PETase^{A} – Generation 1

The crystal structure of the wildtype *Ps*PETase in complex with a substrate analogue (HEMT)[34] displays W185 in three different conformations. This residue is directly interacting with the HEMT moiety, but because HEMT is a small molecule, the structure does not reveal other residues that might be involved in binding the PET substrate. To identify these residues, we performed a model of a Michaelis complex using a 8mer-PET polymer as a substrate (Supplementary Figure S2). Our model indicated that in addition to the interactions with W185, the 8mer-PET polymer is also interacting with residues in the β6-β7 loop (preceded by W185). We performed molecular dynamics simulations of various substitutions at position 186 and found a strong dependence of the flexibility of the sidechain of W185 and the β6-β7 loop on the size of residue 186 (Supplementary Figure S3).

The beneficial effect of the flexibility of W185 and the loops in the active site with the PET hydrolytic activity has been also highlighted by Chen et al.[35] and Crnjar et al.[36] when studying the double mutant S214H/I218F. Based on the MD simulations, we mutated residue D186 to alanine, the residue that was predicted to confer the highest flexibility to the wobbly tryptophan and the β6-β7 loop. The PETase variant D186A (PETase^{A}) exhibited an increase in melting temperature of ~10 °C while at the same time retaining a high level of activity up even at 50 °C. In the 1.6 Å crystal structure of our variant Combi-PETase (Figure 2), we refined W185 and observed that the modelled density around the sidechain of W185 is not completely supported by an occupancy of 1, as well as additional density adjacent but not connected to this residue. However, the additional density was not enough to confidently model a second conformation as observed in previous structures.[37][34] Together with the high B-factors on the atoms of W185, it does suggest that W185 is in fact flexible (Supplementary Figure S6A).

D186 is not conserved in other cutinase enzymes and is most commonly a histidine in thermostable homologs, so the single mutant of *Ps*PETase D186A had not been explored before. The substitution D186H alone does not provide better activity but it led to the development of ThermoPETase[11] which served as scaffold for developing other variants like

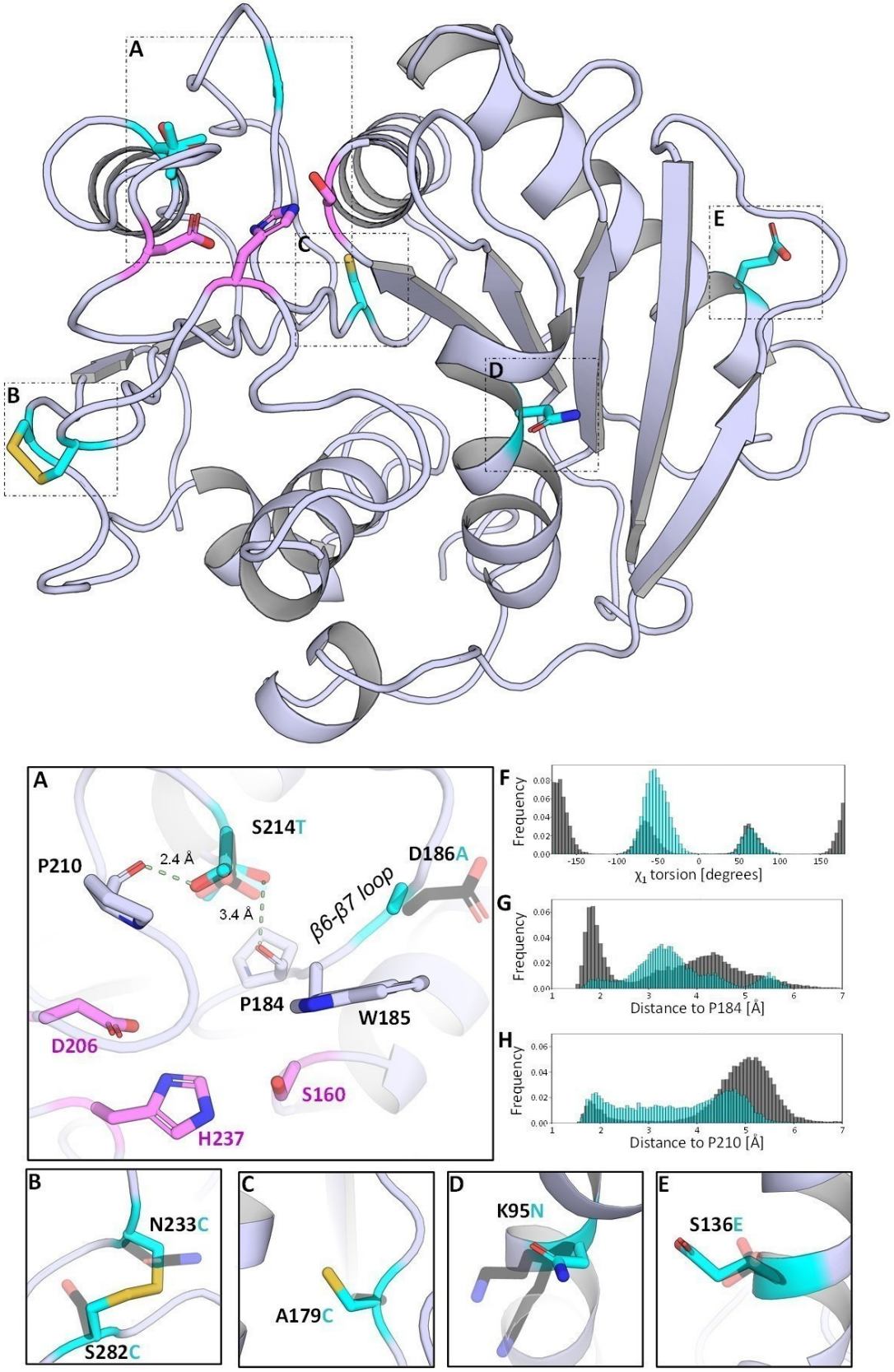

Figure 2. Crystal structure of Combi-PETase. The catalytic triad of S160, D206, and H237 are coloured in magenta. The mutations of interest in this variant are shown in cyan. Insets to highlight the mutations labelled **A**–**E** are shown below the main structure with the same colouring scheme, and with the corresponding WT *Ps*PETase residues shown in semi-transparent black. **F**–**H** Population histogram from the molecular dynamics simulation of wild type (black) vs. Combi-PETase (cyan). The S214T mutation changes the orientation of the residue (χ1 angle) breaking the hydrogen bond interaction with P184. The distances are measured between the hydrogen and the backbone oxygen atoms.

HotPETase[24] and FAST-PETase.[13] This finding aligns with our previous work where the D186S substitution, also predicted to increase the flexibility of the loop and of the wobbly tryptophan (Supplementary Figure S3), yielded a 9 °C improvement in the enzyme's thermostability.[23] Other substitutions (e.g., D186I, D186F, D186 L or D186 V), although being tolerated, led to reduced enzymatic activity,[11] in agreement with the predicted reduced flexibility. Recently, using a semi-saturation mutagenesis experiment, Yin et al. identified the double variant D186A/S121P. Because the crystal structure of the S121P/D186A double mutant could not resolve various conformations of W185 side chain, the authors explained the increased activity was caused by a reduction in the flexibility.[38] However, the authors did not note that this is also common in other crystal structures of *Ps*PETase variants, and that the different conformations of the so-called wobbly tryptophan W185 is not always resolved in multiple conformations. Nailing down all the possible conformations is difficult- seeing that density is missing is easy.

PETase^{ACC} – Generation 2

To further improve the thermal stability of our PETase^{A} variant, we introduced a third disulfide bridge using the N233C and S282C mutations. The design of this disulfide bridge was based on the work of Then et al., who identified a stabilizing calcium binding site in *Tf*Cut2, a homolog enzyme with 51 % sequence similarity of PETase.[39] By engineering a disulfide bridge in that position, the authors mimicked the effect of calcium binding and increased the Tm of *Tf*Cut2 by 24.9 °C.[40] Similar substitutions were performed on Cut190,[41] LCC,[42] and ThermoPETase.[11] Based on a structural alignment between *Tf*Cut2 and PETase^{A}, the equivalent disulfide bridge was engineered between residues N233 and S282. The triple mutant PET^{ACC} displayed a cooperative effect on the thermal stability elevating the melting temperature by another 11.4 °C (to 64.7 °C). The increased melting temperature of PETase^{ACC} allows a much higher activity compared to PETase^{A} at a reaction temperature of 50 °C. The formation of the disulfide bond between N233C and S282C was confirmed to be present and fully occupied in the electron density of the Combi-PETase structure (Supplementary Figure S6C) and the structure of the PETase^{ACC} (PDB accession code 8VEL).

PETase^{ACCCET} – Generation 3

Further attempts to improve the thermal stability of our PETase^{ACC} variant by rational design only led to modest improvements. Individually, the A179C, S136E and S214T (CET) mutations each increased melting temperature of PETase^{ACC} by ca. 3.2 °C, 0.9 °C and 2.1 °C respectively (Supplementary Table S3). However, the effect of these mutations was additive and the combined mutant PETase^{ACCCET} displayed a Tm of 67.8 °C (Figure 1A, Table 1), sufficient to increase the optimal reaction temperature to 60 °C.

The A179C variant fills a hydrophobic cavity in the core of the enzyme, a strategy that is commonly used to improve the thermal stability of mesophilic enzymes.[41] This effect is apparent in the density around residue A179C in the crystal structure of Combi-PETase (Supplementary Figure S6D).

The mutant S136E has a small effect on the thermal stability of the enzyme as measured by DSF, but it also showed a 1.3-fold increase in hydrolytic activity compared to our PETase^{ACC} variant and was compatible with the other mutations, so it was retained for future generations. In the crystal structure we do not see the direct formation of any new salt bridge by the S136E substitution, so the effect may be due to a transient intraprotein interaction or to an improvement in enzyme-solvent interactions.

The S214T variant increased the enzymatic activity by 12 % (Supplementary Table S3). Both the crystal structure of Combi-PETase (this work) and of the wild type (PDB 6EQE)[43] resolve the sidechain of residue 214 in three different orientations with similar occupancies. Molecular dynamics simulations show that in the wild type, S214 (located in β7-α4 loop) preferably makes a hydrogen bond with the carbonyl of P184, located at the start of the β6-β7 loop, while the mutation to threonine (T214) breaks this interaction (Figure 2F and G). This can enhance the flexibility of the β6-β7 loop and the binding site, explaining the increased activity of this variant. Both A179C and S214T are newly discovered mutations, while S136E has been previously shown present similar beneficial effects on the wild type sequence.[44]

PETase^{ACCCETN} – Generation 4

In a previous publication we performed an Ancestral Sequence Reconstruction (ASR) experiment on the wild type *Ps*PETase, in which identified some ancestor sequences that showed improved thermostability.[20] Continuing from this, we integrated and tested several of the ASR designs into our PETase^{ACCCET} variant (Supplementary Table S4) and identified the K95N mutation which exhibited a further increase in thermal stability (Tm = 70.4 °C) and a 12 % increase in terms of enzymatic activity. Two directed evolution experiments rendered variants that included the K95N mutation: HOT-PETase[21] and PETaseTM,[43] (with 21 and 2 mutations respectively).

Combining Machine Learning/AI Mutations to the PETase^{ACCCETN}

A new variant (FAST-PETase) has recently been developed using a ML-based enzyme engineering method (MutCompute)[13] and based on the ThermoPETase variant. The authors predicted and tested 159 mutations and identified three of them (N233K, R224Q and S121E) that when added to the ThermoPETase (D186H/R280A) yielded a variant with high activity at an optimal temperature of 50 °C. From the FAST-PETase mutations, the N233K mutant is of particular interest, because introducing this single point mutation on other homologous PET-degrading enzymes also produces enzymes with higher degradation rates.

Thus, it appears that this mutation is transferable to related enzymes. We introduced the N233K mutant into our Combi-PETase, noting that this mutation would break the engineered disulfide bridge between residue N233C and S282C. Because it is difficult to compare the results from the literature given that the reaction conditions and the substrates often differ,[21] we decided to order, express, purify and test the FAST-PETase sequence as from the literature but using our activity assay and substrates.[13] The new variant derived from FAST-PETase and Combi-PETase (namely PETase^{AKCETN}) showed a modest Tm decrease to 67.5 °C compared to Combi-PETase and a reduction of 10 °C of the optimum temperature back to 50 °C, same as the FAST-PETase variant. (Figure 1A and 1C, Table 1). The activity of PETase^{AKCETN} at 50 °C is the same as Combi-PETase at the same temperature but lower than the Combi-PETase at 60 °C. However, the yield of the PETase^{AKCETN} variant is much higher (Figure 1B, Table 1).

Assessing the Enzyme's Suitability for Industrial Applications

Due to higher activity and protein yields, we evaluated the suitability of the Combi-PETase and PETase^{AKCETN} variants for industrial applications. For these two variants, we performed long-term reaction experiments at high temperatures and high enzyme concentrations, and we also tested the residual activity of Combi-PETase against a high-crystalline PET substrate.

Figure 3 shows the enzymes' activity at 50 and 60 °C for up to 28 hours using FAST-PETase as a control. While at 50 °C, all these enzymes perform similarly after either 2 or 28 hours (Figure 3A, and Supplementary Figure S4), at 60 °C Combi-PETase performs better than PETase^{AKCETN}, which in turn is better than FAST-PETase.

Wild type *Ps*PETase has been noted to show a concentration inhibition effect when the enzyme's concentration exceeds 150 nM.[6] Although the reason for this inhibition is not fully understood, this is a problem for industrial applications. Avilan et al. has shown that it is also present in other mesophilic enzymes and that it can be improved using protein engineering to increase the thermal stability, by adding additives to the reaction (e.g. DMSO), or by modifying the substrate (increasing the polymer surface area).[45] HotPETase, a variant generated by a directed mutagenesis approach,[24] is an example of a highly thermostable variant that shows reduced inhibition by enzyme concentration. This effect is also displayed in our Combi-PETase, where we observe at least a 4-fold increase in the optimal enzyme concentration for the reaction (to ~800 nM, Figure 3C).

*Ps*PETase has been discovered to naturally break down low crystalline PET (lc-PET). However, high crystalline PET (hc-PET) is a prevalent waste product that is difficult to break down by all known PETases. To determine the effect of the crystallinity of the substrate on the reaction rate of our Combi-PETase, we tested the enzyme against both hc-PET (post-consumer Coca-Cola bottle, ca. 45% crystallinity)[46] and lc-PET (powdered GoodFellow PET film, amorphous). We measured the degradation products (TPA and MHET) over 28 hours using UPLC (Figure 4). As usual for all PET hydrolases, lc-PET is more susceptible to breakdown by Combi-PETase than hc-PET, resulting in a total of 29 mM and 19 mM of total released products respectively. However, this means that the Combi-PETase retains 65% of the activity against hc-PET, which is very high compared to other PETase enzymes.[19,47] Indeed, LCC^{IGGA} variant retains between 25–35% activity when reacting with microparticles ($\leq$250 μm) of 32–35% crystalline PET.[20] Most PET degrading enzymes also show less than 50% activity against PET film substrates with 13–23% crystallinity.[17]

Conclusions

We combined different enzyme engineering approaches; structure-based rational design, ancestral sequence reconstruction and mutations from AI/machine learning to develop a new variant of *Ps*PETase. We found the biggest improvements in the enzyme's properties from the early generations using a rational-based design. By the second generation (PETase^{ACC}), the melting

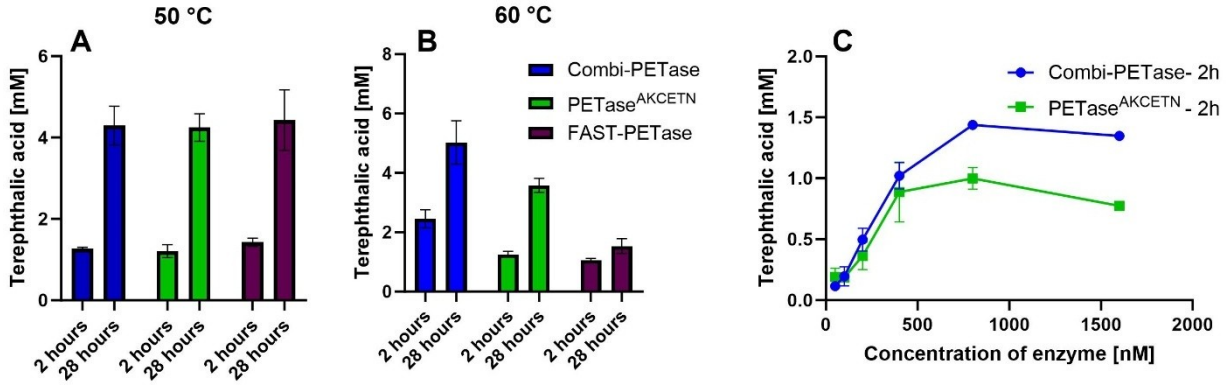

Figure 3. Enzymatic activity of Combi-PETase, PETase^{AKCETN} and FAST-PETase at **A)** 50 and **B)** 60 °C. All reactions were performed using 800 nM enzyme and 90 mg of hc-PET in 0.5 mL bicine buffer at pH 9.0 and agitating at 1000 rpm. Samples were taken from the reaction mixture at times 2 h and 28 h. **C)** Enzymatic activity of Combi-PETase and PETase^{AKCETN} variants incubated at 50 °C with varying concentration of enzyme 50–1600 nM, using 90 mg of hc-PET substrate in 0.5 mL bicine buffer at pH 9.0 and agitating at 1000 rpm. In all cases the enzymatic activity was measured using the fluorometric assay as explained in the methods section and in reference 23.

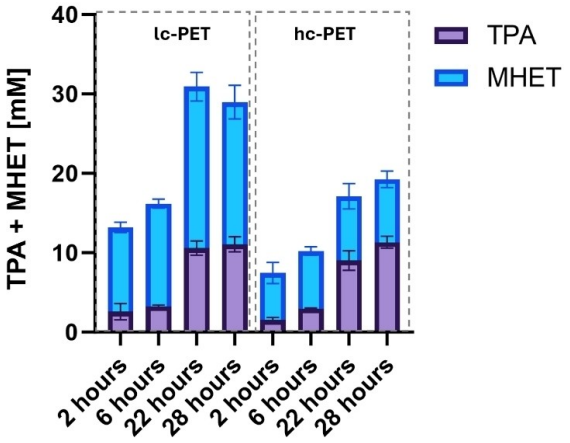

Figure 4. lc-PET and hc-PET (90 mg) using 2 μM Combi-PETase (PETase^{ACCCETN}) enzyme incubated for 2, 6, 22 and 28 hours determining the amount of TPA and MHET. Both reactions were performed in three replicates each and incubated at 60 °C for one hour agitating at 1000 rpm analysed using UPLC.

temperature was increased by 22 °C. Further generations also based on rational design improved the thermostability by another 4 °C and the activity by 43% but further improvements were difficult. A new mutation based on the ASR method further improved the enzyme's stability by another 2 °C and increased the activity by 10%. The SDS-PAGE gel shows that the amount of soluble Combi-PETase protein was qualitatively increased with respect to the wild type *Ps*PETase (Figure S8), while the amount of purified Combi-PETase protein was increased by 25-fold (Figures S9 and S10). The increased solubility of Combi-PETase is also reflected in the decrease in the concentration-dependent inhibition, which means that the Combi-PETase can be efficiently used at 800 nM concentration instead of $<$150 nM for the wild type *Ps*PETase. Based on AI methods, the N233K mutation was proposed. Introducing this mutation to the Combi-PETase variant improved the protein yields, but it also reduced its thermostability and activity. Therefore, it was not included in our final variant.

Each technique contributed to the advancement of the engineered Combi-PETase (PETase^{ACCCETN}). We highlight the importance of applying these approaches simultaneously as each of them has its strengths and limitations. The biggest improvements were based on understanding the structure of the protein, the substrate binding mode, and the mechanism of action. ASR and AI-based tools were more effective in predicting the impact of remote mutations on the enzyme's properties, which were challenging to foresee with structure-based protein engineering. Although we may not fully understand how remote mutations affect the protein's biophysics in detail, their beneficial effects are evident.

Overall, this study demonstrates a successful example of a combinatorial enzyme engineering experiment, using structure-, bioinformatics- and AI-based strategies. We have engineered the Combi-PETase variant to perform better in terms of protein yields, thermostability, activity, tolerance to high enzyme concentration and longer reaction times; compared to the wildtype *Ps*PETase and most of the published PETase enzymes. It is highly active over a range of temperatures and can hydrolyze not only lc-PET but also hc-PET with high efficiency. These are all desirable biophysical and biochemical properties when considering the enzyme for industrial applications. However, we have not upscaled the process or directly compared the Combi-PETase under standardized industry-like conditions against other PETase enzymes as done for other variants.[21]

Materials and Methods

Protein Expression and Purification

The engineered variants were synthesized at GenScript (containing a C-terminal His-tag) in a modified expression vector pET-43.1a (+) from Novagen (Supplementary Figure S1). The proteins were expressed and purified as previously described. E. coli BL21-(DE3) was used for expression and induced at OD600 ~0.8 by addition of isopropyl β-D-1-thiogalactopyranoside (IPTG) to a final concentration of 0.1 mM. The cells were grown in 0.5 or 1 L TB medium and further incubated for ~18 h at 16 °C and agitated at 180 rpm. Afterwards, the cells were harvested by centrifugation at 6,000×g for 10 minutes at 4 °C and resuspended in lysis buffer (1x PBS, 350 mM NaCl, 10% (w/v) glycerol, 45μg lysozyme, 2 mM $MgCl_2$, and 20 mM imidazole) and lysed by sonication. The lysed cells were harvested at 25'000 g for 25 minutes. The soluble fraction of the variants was purified on an ÄKTAxpress (GE Healthcare) using a 1 mL HisTrap FF column (GE Healthcare), followed by automated peak injection onto a HiLoad Superdex 200 16/60 prep grade column (GE Healthcare). Unbound protein was washed off with IMAC wash buffer (1× PBS, 350 mM NaCl, 10% w/v glycerol, 20 mM imidazole) and the bound proteins were eluted using an IMAC elution buffer (1x PBS, 350 mM NaCl, 10% w/v glycerol, 500 mM imidazole). The proteins were run over a Superdex S200 size exclusion column with SEC buffer (50 mM bicine, 100 mM NaCl, pH 9.0), concentrated using a 10,000 MWCO concentrator (Amicon) and SDS-PAGE was run to assess the protein purity. Protein concentration was determined by nanodrop using ProtParam calculated (Expasy) extinction coefficient at 280 nm.[46] The protein was snap-frozen in liquid nitrogen and stored in 100 μL aliquots.

Thermostability Measurement

The thermal stability of the purified variants was determined with differential scanning fluorimetry (DSF). The protein was diluted to a concentration of 40 μg/mL in (50 mM bicine, 100 mM NaCl, pH 9.0). 20 μL was pipetted into a 96-well white PCR plate (ThermoFisher Scientific) and added 0.3 μL 75× SYPRO orange dye using nano-dispensing robots (Art Robbins Phoenix). The melting temperature shift was measured using the FRET channel of a CFX96 qPCR instrument (Bio-rad) from 20–100 °C. All protein samples were set up in six replicates.

Enzymatic Activity of Engineered PET Hydrolases

The PET degradation reactions were prepared with 90 mg ground hc-PET particles (< 5 mm) from a Coca-cola bottle or micronized lc-PET (≤500 μm particles GoodFellow PET film, amorphous) in a 500 μl buffer (50 mM bicine 100 mM NaCl, pH 9). The reaction was initiated by adding 500 nM to 1600 nM enzymes and incubated for 1 to 28 hours at the enzyme's optimal temperature and 1000 rpm on an Eppendorf Thermo-Mixer. To determine the optimal temperature, experiments between 30–70 °C were performed. The hydrolysis reactions were stopped at 95 °C for 10 minutes and the microplastic was centrifuged at 11,000 rpm for two minutes. The enzymatic activity of the designed variants was measured as previously described.[23] 10-100 μL of the reaction mixture was pipetted into a black 96-well plate and the volume was adjusted to 100 μL with bicine buffer. The reaction to produce fluorescent 2-hydroxy terephthalate (HOTP), was initiated by adding 25 μL of 5 mM EDTA and 25 μL of 5 mM $FeSO_4$ with a multichannel pipet. Finally, 25 μL of 2% H_2O_2 was added by mixing the reaction mixture. Subsequently, the reaction mixture was incubated for 60 min at room temperature before the fluorescence was measured with a plate reader from CLARIOstar BMG-Labtech Australia (λ_{ex} = 320 nm, and λ_{em} = 420 nm). We interpolated the concentration of TPA based on a calibration curve of terephthalic acid (TPA) between 0–500 μM. The PET hydrolase variants were compared to the previous variants as a reference to determine whether the enzymatic activity has increased, and experiments were performed in triplicate.

UPLC Analysis of PET Hydrolysis

To determine TPA and MHET concentrations, we employed Ultra Performance Liquid Chromatography (UPLC) using an Acquity UPLC i-Class equipped with a QDa performance mass detector (Waters). The chromatogram extraction was conducted at a wavelength of 254 nm. The UPLC system utilized an Acquity UPLC BEH C18 column (50×2.1 mm, 1.7 μm particle size). The mobile phases employed were as follows: mobile phase A consisted of 99.9% Milli-Q Water + 0.1% formic acid, and mobile phase B was composed of 99.9% Acetonitrile + 0.1% formic acid. The flow rate was maintained at 0.400 mL/min, and a sample volume of 1 μL was injected three times for each analysis. Following sample injection, the mobile phase composition transitioned from 95% A to 100% B over a 4.50-minute interval and remained at 100% B for 1 minute. Subsequently, it was changed back to 95% A over 0.5 minutes and held at that composition for an additional 1 minute. To interpolate the concentrations of TPA and MHET, we prepared calibration curves ranging from 0 to 500 μM by utilising the mass of each compound.

Protein Crystallisation and Structure Determination

Crystals of the PETase variants were grown by vapour diffusion in MRC 2 sitting-drop plates (Swissci) setting up drops at a 1:1 ratio with 150 nl of protein and 150 nl of mother liquor using the Phoenix Crystal (Art Robbins) liquid handling platform with crystallisation conditions described in Supplementary Table S8. Crystals grew after a couple of days and prior to flash cooling in liquid nitrogen were cryoprotected with a final concentration of 15% glycerol added to the reservoir before overlaying onto the drop. Diffraction experiments were carried out at the Australian Synchrotron MX2 beamline[48] under nitrogen vapor at 100K and a wavelength of 0.974 Å. Data reduction was carried out with XDS[48] for indexing and integration followed by scaling and merging with Aimless.[49] Automated implementation of the same programs was utilised with autoPROC.[50] Molecular replacement was carried out with Phaser[51] via a model derived from the PDB ID 6EQE.[43] The model was iteratively built and refined with Coot 0.8.9[51] and Refmac 5.7[52] (Combi-PETase/ PETase^{ACCCETN}) via the CCP4i2 user interface,[53] Phenix (PETase^{ACC}),[54] or autoBUSTER (PETase^{ACCC} and PETase^{ACCE}).[55] Statistics for structure solution and refinement are presented in Supplementary Table S7.

Protein Modelling and Molecular Dynamics Simulations

A model of the 8mer-PET substrate in complex with the wild type *Ps*PETase enzyme was build using the 6EQE model as starting structure.[43] The substrate was modelled in a step-wise manner. First, a flexible molecule of Mono-(2-hydroxyethyl)terephthalic acid (MHET) was docked in the active site (using residue S160 as the centre of the box). Then, one by one, new moieties of MHET were added to both ends of the first molecule until the 8mer-PET substrate was finished. At each step, a 1μs molecular dynamics simulation was performed to relax the system, applying a distance harmonic constraint between the carbonyl oxygen atom of the first molecule docked and the backbone nitrogen atoms of residues Y87 and M161 (the residues defining the tetrahedral oxoanionic binding site) to ensure that the substrate remained in the active site. Finally, 1μs MD simulation of the 8mer-PET substrate was performed without any constraint. Alignment of the modelled complex with the crystal structure of *Ps*PETase in complex with MHET (PDB 7XTW)[56] shows very good agreement in the docking pose of the substrate. The docking of the first MHET molecule was performed using AutoDock4 and the molecular dynamics simulations were performed using the CUDA version of AMBER20.[57,58,59,60] The force field used for the protein was ff14SB[61] and the substrate was modelled using the gaff2 forcefield, reducing the substrate-substrate van-der-Waals self-interactions by 50% to avoid aggregation. The system was solvated in a TIP3P water model[62] using periodic boundary conditions with a 12 Å distance from the protein. An 80 mM concentration of NaCl was used ensuring charge neutrality of the system. van der Waals and electrostatic interactions were capped at 12 Å using a smooth potential while a PM3

implementation[63] was used to describe the long-range electrostatic interactions. The initial structure was relaxed using an energy minimization protocol using a steepest-descent and a Newton-Raphson algorithms. The temperature was increased to 300K in a 15 ns MD simulation in the NPT ensemble and then the production run performed in the NVT ensemble coupling the system to a thermostat. All molecular dynamics simulations were performed using a timestep of 2 fs, with a constraint on the hydrogen atoms. The MD simulations of the wild type enzyme in complex with the 8mer-PET substrate were extended for 1μs. The MD simulations of the mutants to produce Figure S3 and of Combi-PETase to produce Figure 2F–H were extended for 2μs. The analysis of the MD simulations was performed using AMBER-Tools, VMD[64] and in-house scripts.

Mutations based on the Ancestral Sequence Reconstruction bioinformatics approach were chosen from our previous work[23] while AI-based mutations were based on published work.[13]

Supporting Information

The supplementary information is available at ChemBioChem. The structures of PETase^{ACC}, (8VEK) PETase^{ACCCC}, (8VEL) PETase^{ACCCE}, (8VEM), and CombiPETase/PETase^{ACCCETN} (8VE9) have been deposited to the Protein Data Bank. The data that support the findings of this study are available from the corresponding author upon reasonable request.

Acknowledgements

All crystallisation experiments were carried out at CSIRO's C3 and BBC facilities, Melbourne, Australia. This research was undertaken in part using the MX2 beamline at the Australian Synchrotron, part of ANSTO, and made use of the Australian Cancer Research Foundation (ACRF) detector. We acknowledge Lesley Pearce for help with optimising our purification process using the ÄKTAxpress machines. Stewart Nuttall for the original plasmid design of pET43 and the CSIRO Ending Plastic Waste mission. All UPLC experiments were performed in CSIRO HPLC/UPLC facility led by Megan Kruger.

Conflict of Interests

The authors declare no conflict of interest, they acknowledge a previous provisional patent application for Hydrolase variants (WO2022104434A1).

Data Availability Statement

The data that support the findings of this study are available from the corresponding author upon reasonable request.

Keywords: Ancestral sequence reconstruction · Biocatalysis · Machine learning · PET hydrolase (PETase) · Protein engineering

[1] M. MacLeod, H. P. H. Arp, M. B. Tekman, A. Jahnke, *Science* **2021**, *373*, 61–65.
[2] C. Campanale, C. Massarelli, I. Savino, V. Locaputo, V. F. Uricchio, *Int. J. Environ. Res. Public Health* **2020**, *17*, *1212*.
[3] R. Geyer, J. R. Jambeck, K. L. Law, *Sci. Adv.* **2017**, *3*, e1700782.
[4] A. Singh, N. A. Rorrer, S. R. Nicholson, E. Erickson, J. S. Desveaux, A. F. T. Avelino, P. Lamers, A. Bhatt, Y. Zhang, G. Avery, L. Tao, A. R. Pickford, A. C. Carpenter, J. E. McGeehan, G. T. Beckham, *Joule* **2021**, *5*, 2479–2503.
[5] R.-J. Müller, H. Schrader, J. Profe, K. Dresler, W.-D. Deckwer, *Macromol. Rapid Commun.* **2005**, *26*, 1400–1405.
[6] S. Yoshida, K. Hiraga, T. Takehana, I. Taniguchi, H. Yamaji, Y. Maeda, K. Toyohara, K. Miyamoto, Y. Kimura, K. Oda, *Science* **2016**, *351*, 1196–1199.
[7] H. T. Tan, M. F. Chek, S. Z. Neoh, S. L. Ang, S. Yoshida, T. Hakoshima, K. Sudesh, *Polym. Degrad. Stab.* **2022**, *206*, 110160.
[8] R. Fujiwara, R. Sanuki, H. Ajiro, T. Fukui, S. Yoshida, *Sci. Rep.* **2021**, *11*, 19991.
[9] S. Sulaiman, S. Yamato, E. Kanaya, J. J. Kim, Y. Koga, K. Takano, S. Kanaya, *Appl. Environ. Microbiol.* **2012**, *78*, 1556–1562.
[10] C. M. Silva, F. Carneiro, A. O'Neill, L. P. Fonseca, J. S. M. Cabral, G. Guebitz, A. Cavaco-Paulo, *J. Polym. Sci. Part A* **2005**, *43*, 2448–2450.
[11] H. F. Son, I. J. Cho, S. Joo, H. Seo, H.-Y. Sagong, S. Y. Choi, S. Y. Lee, K.-J. Kim, *ACS Catal.* **2019**, *9*, 3519–3526.
[12] Y. Cui, Y. Chen, X. Liu, S. Dong, Y. E. Tian, Y. Qiao, R. Mitra, J. Han, C. Li, X. Han, W. Liu, Q. Chen, W. Wei, X. Wang, W. Du, S. Tang, H. Xiang, H. Liu, Y. Liang, K. N. Houk, B. Wu, *ACS Catal.* **2021**, *11*, 1340–1350.
[13] H. Lu, D. J. Diaz, N. J. Czarnecki, C. Zhu, W. Kim, R. Shroff, D. J. Acosta, B. R. Alexander, H. O. Cole, Y. Zhang, N. A. Lynd, A. D. Ellington, H. S. Alper, *Nature* **2022**, *604*, 662–667.
[14] K. Chen, Y. Hu, X. Dong, Y. Sun, *ACS Catal.* **2021**, *11*, 7358–7370.
[15] L. Dai, Y. Qu, J. W. Huang, Y. Hu, H. Hu, S. Li, C. C. Chen, R. T. Guo, *J. Biotechnol.* **2021**, *334*, 47–50.
[16] M. Furukawa, N. Kawakami, K. Oda, K. Miyamoto, *ChemSusChem* **2018**, *11*, 4018–4025.
[17] T. B. Thomsen, K. Almdal, A. S. Meyer, *New Biotechnol.* **2023**, *78*, 162–172.
[18] R. Wei, D. Breite, C. Song, D. Gräsing, T. Ploss, P. Hille, R. Schwerdtfeger, J. Matysik, A. Schulze, W. Zimmermann, *Adv. Sci.* **2019**, *6*, 1900491.
[19] S. Weinberger, K. Haernvall, D. Scaini, G. Ghazaryan, M. T. Zumstein, M. Sander, A. Pellis, G. M. Guebitz, *Green Chem.* **2017**, *19*, 5381–5384.
[20] R. K. Brizendine, E. Erickson, S. J. Haugen, K. J. Ramirez, J. Miscall, D. Salvachúa, A. R. Pickford, M. J. Sobkowicz, J. E. McGeehan, G. T. Beckham, *ACS Sustainable Chem. Eng.* **2022**, *10*, 9131–9140.
[21] G. Arnal, J. Anglade, S. Gavalda, V. Tournier, N. Chabot, U. T. Bornscheuer, G. Weber, A. Marty, *ACS Catal.* **2023**, *13*, 13156–13166.
[22] M. A. Spence, J. A. Kaczmarski, J. W. Saunders, C. J. Jackson, *Curr. Opin. Struct. Biol.* **2021**, *69*, 131–141.
[23] Y. Joho, V. Vongsouthi, M. A. Spence, J. Ton, C. Gomez, L. L. Tan, J. A. Kaczmarski, A. T. Caputo, S. Royan, C. J. Jackson, A. Ardevol, *Biochemistry* **2023**, *62*, 437–450.
[24] E. L. Bell, R. Smithson, S. Kilbride, J. Foster, F. J. Hardy, S. Ramachandran, A. A. Tedstone, S. J. Haigh, A. A. Garforth, P. J. R. Day, C. Levy, M. P. Shaver, A. P. Green, *Nature Catalysis* **2022**, *5*, 673–681.
[25] R. Shroff, A. W. Cole, D. J. Diaz, B. R. Morrow, I. Donnell, A. Annapareddy, J. Gollihar, A. D. Ellington, R. Thyer, *ACS Synth. Biol.* **2020**, *9*, 2927–2935.
[26] V. Gligorijević, P. D. Renfrew, T. Kosciolek, J. K. Leman, D. Berenberg, T. Vatanen, C. Chandler, B. C. Taylor, I. M. Fisk, H. Vlamakis, R. J. Xavier, R. Knight, K. Cho, R. Bonneau, *Nat. Commun.* **2021**, *12*, 3168.
[27] H. F. Son, S. Joo, H. Seo, H.-Y. Sagong, S. H. Lee, H. Hong, K.-J. Kim, *Enzyme Microb. Technol.* **2020**, *141*, 109656.
[28] E. Z. L. Zhong-Johnson, C. A. Voigt, A. J. Sinskey, *Sci. Rep.* **2021**, *11*.
[29] Y. Gumulya, J.-M. Baek, S.-J. Wun, R. E. S. Thomson, K. L. Harris, D. J. B. Hunter, J. B. Y. H. Behrendorff, J. Kulig, S. Zheng, X. Wu, B. Wu, J. E. Stok, J. J. De Voss, G. Schenk, U. Jurva, S. Andersson, E. M. Isin, M. Bodén, L. Guddat, E. M. J. Gillam, *Nature Catalysis* **2018**, *1*, 878–888.
[30] N. M. Hendrikse, G. Charpentier, E. Nordling, P.-O. Syrén, *FEBS J.* **2018**, *285*, 4660–4673.
[31] S. Meng, Z. Li, P. Zhang, F. Contreras, Y. Ji, U. Schwaneberg, *Chin. J. Catal.* **2023**, *50*, 229–238.

[32] R. Jiang, L. Shang, R. Wang, D. Wang, N. Wei, *Environ. Sci. Technol. Lett.* **2023**, *10*, 557–564.
[33] A. Gupta, S. Agrawal, *J. Emerg. Inv.* **2023**, *6*, 1.
[34] X. Han, W. Liu, J.-W. Huang, J. Ma, Y. Zheng, T.-P. Ko, L. Xu, Y.-S. Cheng, C.-C. Chen, R.-T. Guo, *Nat. Commun.* **2017**, *8, 2106*.
[35] C.-C. Chen, X. Han, X. Li, P. Jiang, D. Niu, L. Ma, W. Liu, S. Li, Y. Qu, H. Hu, J. Min, Y. Yang, L. Zhang, W. Zeng, J.-W. Huang, L. Dai, R.-T. Guo, *Nature Catalysis* **2021**, *4*, 425–430.
[36] A. Crnjar, A. Griñen, S. C. L. Kamerlin, C. A. Ramírez-Sarmiento, *ACS Org, Inorg. Au* **2023**, *3*, 109–119.
[37] S. Joo, I. J. Cho, H. Seo, H. F. Son, H.-Y. Sagong, T. J. Shin, S. Y. Choi, S. Y. Lee, K.-J. Kim, *Nat. Commun.* **2018**, *9*, 382.
[38] Q. Yin, J. Zhang, S. Ma, T. Gu, M. Wang, S. You, S. Ye, R. Su, Y. Wang, W. Qi, *Green Chem.* **2023**, *26*, 2560–2570.
[39] M. Furukawa, N. Kawakami, A. Tomizawa, K. Miyamoto, *Sci. Rep.* **2019**, *9*.
[40] J. Then, R. Wei, T. Oeser, A. Gerdts, J. Schmidt, M. Barth, W. Zimmermann, *FEBS Open Bio* **2016**, *6*, 425–432.
[41] M. Oda, Y. Yamagami, S. Inaba, T. Oida, M. Yamamoto, S. Kitajima, F. Kawai, *Appl. Microbiol. Biotechnol.* **2018**, *102*, 10067–10077.
[42] V. Tournier, C. M. Topham, A. Gilles, B. David, C. Folgoas, E. Moya-Leclair, E. Kamionka, M. L. Desrousseaux, H. Texier, S. Gavalda, M. Cot, E. Guémard, M. Dalibey, J. Nomme, G. Cioci, S. Barbe, M. Chateau, I. André, S. Duquesne, A. Marty, *Nature* **2020**, *580*, 216–219.
[43] H. P. Austin, M. D. Allen, B. S. Donohoe, N. A. Rorrer, F. L. Kearns, R. L. Silveira, B. C. Pollard, G. Dominick, R. Duman, K. El Omari, V. Mykhaylyk, A. Wagner, W. E. Michener, A. Amore, M. S. Skaf, M. F. Crowley, A. W. Thorne, C. W. Johnson, H. L. Woodcock, J. E. McGeehan, G. T. Beckham, *Proc. Natl. Acad. Sci. USA* **2018**, *115*, E4350–E4357.
[44] A. Rennison, J. R. Winther, C. Varrone, *Polymers (Basel).* **2021**, *13, 3884*.
[45] L. Avilan, B. R. Lichtenstein, G. König, M. Zahn, M. D. Allen, L. Oliveira, M. Clark, V. Bemmer, R. Graham, H. P. Austin, G. Dominick, C. W. Johnson, G. T. Beckham, J. E. McGeehan, A. R. Pickford, *ChemSusChem* **2023**, *16*, e202202277.
[46] S. Giraldo-Narcizo, N. Guenani, A. M. Sánchez-Pérez, A. Guerrero, *ChemBioChem* **2023**, *24*, e202200503.
[47] M. A. M. E. Vertommen, V. A. Nierstrasz, M. v. d. Veer, M. M. C. G. Warmoeskerken, *J. Biotechnol.* **2005**, *120*, 376–386.
[48] D. Aragão, J. Aishima, H. Cherukuvada, R. Clarken, M. Clift, N. P. Cowieson, D. J. Ericsson, C. L. Gee, S. Macedo, N. Mudie, S. Panjikar, J. R. Price, A. Riboldi-Tunnicliffe, R. Rostan, R. Williamson, T. T. Caradoc-Davies, *J. Synchrotron Radiat.* **2018**, *25*, 885–891.
[49] P. R. Evans, G. N. Murshudov, *Acta Crystallogr. Sect. D* **2013**, *69*, 1204–1214.
[50] C. Vonrhein, C. Flensburg, P. Keller, A. Sharff, O. Smart, W. Paciorek, T. Womack, G. Bricogne, *Acta Crystallogr. Sect. D* **2011**, *67*, 293–302.
[51] P. Emsley, B. Lohkamp, W. G. Scott, K. Cowtan, *Acta Crystallogr. Sect. D* **2010**, *66*, 486–501.
[52] G. N. Murshudov, P. Skubak, A. A. Lebedev, N. S. Pannu, R. A. Steiner, R. A. Nicholls, M. D. Winn, F. Long, A. A. Vagin, *Acta Crystallogr. Sect. D* **2011**, *67*, 355–367.
[53] L. Potterton, J. Agirre, C. Ballard, K. Cowtan, E. Dodson, P. R. Evans, H. T. Jenkins, R. Keegan, E. Krissinel, K. Stevenson, A. Lebedev, S. J. McNicholas, R. A. Nicholls, M. Noble, N. S. Pannu, C. Roth, G. Sheldrick, P. Skubak, J. Turkenburg, V. Uski, F. von Delft, D. Waterman, K. Wilson, M. Winn, M. Wojdyr, *Acta Crystallogr. Sect. D* **2018**, *74*, 68–84.
[54] P. D. Adams, P. V. Afonine, G. Bunkóczi, V. B. Chen, I. W. Davis, N. Echols, J. J. Headd, L. W. Hung, G. J. Kapral, R. W. Grosse-Kunstleve, A. J. McCoy, N. W. Moriarty, R. Oeffner, R. J. Read, D. C. Richardson, J. S. Richardson, T. C. Terwilliger, P. H. Zwart, *Acta Crystallogr. Sect. D* **2010**, *66*, 213–221.
[55] E. B. G. Bricogne, M. Brandl, C. Flensburg, P. Keller, W. Paciorek, P. Roversi, A. Sharff, O. S. Smart, C. Vonrhein, T. O. Womak, *BUSTER*, Cambridge, United Kingdom: Global Phasing Ltd., **2017**.
[56] Y. Yang, J. Min, T. Xue, P. Jiang, X. Liu, R. Peng, J.-W. Huang, Y. Qu, X. Li, N. Ma, F.-C. Tsai, L. Dai, Q. Zhang, Y. Liu, C.-C. Chen, R.-T. Guo, *Nat. Commun.* **2023**, *14*, 1645.
[57] D. A. Case, H. M. Aktulga, K. Belfon, D. S. Cerutti, G. A. Cisneros, V. W. D. Cruzeiro, N. Forouzesh, T. J. Giese, A. W. Götz, H. Gohlke, S. Izadi, K. Kasavajhala, M. C. Kaymak, E. King, T. Kurtzman, T.-S. Lee, P. Li, J. Liu, T. Luchko, R. Luo, M. Manathunga, M. R. Machado, H. M. Nguyen, K. A. O'Hearn, A. V. Onufriev, F. Pan, S. Pantano, R. Qi, A. Rahnamoun, A. Risheh, S. Schott-Verdugo, A. Shajan, J. Swails, J. Wang, H. Wei, X. Wu, Y. Wu, S. Zhang, S. Zhao, Q. Zhu, T. E. Cheatham, III, D. R. Roe, A. Roitberg, C. Simmerling, D. M. York, M. C. Nagan, K. M. Merz, Jr., *J. Chem. Inf. Model.* **2023**, *63*, 6183–6191.
[58] R. Salomon-Ferrer, A. W. Götz, D. Poole, S. Le Grand, R. C. Walker, *J. Chem. Theory Comput.* **2013**, *9*, 3878–3888.
[59] A. W. Götz, M. J. Williamson, D. Xu, D. Poole, S. Le Grand, R. C. Walker, *J. Chem. Theory Comput.* **2012**, *8*, 1542–1555.
[60] S. Le Grand, A. W. Götz, R. C. Walker, *Comput. Phys. Commun.* **2013**, *184*, 374–380.
[61] J. A. Maier, C. Martinez, K. Kasavajhala, L. Wickstrom, K. E. Hauser, C. Simmerling, *J. Chem. Theory Comput.* **2015**, *11*, 3696–3713.
[62] W. L. Jorgensen, J. Chandrasekhar, J. D. Madura, R. W. Impey, M. L. Klein, *J. Chem. Phys.* **1983**, *79*, 926–935.
[63] P. H. Hünenberger, *J. Chem. Phys.* **2000**, *113*, 10464–10476.
[64] W. Humphrey, A. Dalke, K. Schulten, *J. Mol. Graphics* **1996**, *14*, 33–38.

Manuscript received: January 30, 2024
Revised manuscript received: April 2, 2024
Accepted manuscript online: April 7, 2024
Version of record online: May 2, 2024